Multiphase nonlinear electron plasma waves

Vadim R. Munirov,[1,*] Lazar Friedland,[2] and Jonathan S. Wurtele[1]

[1] *Department of Physics, University of California, Berkeley, California 94720, USA*
[2] *Hebrew University of Jerusalem, Jerusalem 91904, Israel*

(Dated: v1 May 28, 2022; v2 September 18, 2022)

We present a method for constructing multiphase excitations in the generally non-integrable system of warm fluid equations describing plasma oscillations. It is based on autoresonant excitation of nonlinear electron plasma waves by phase locking with small amplitude chirped-frequency ponderomotive drives. We demonstrate the excitation of these multiphase waves by performing fully nonlinear numerical simulations of the fluid equations. We develop a simplified model based on a weakly nonlinear analytical theory by applying Whitham's averaged Lagrangian procedure. The simplified model predictions are in good agreement with the results from the warm fluid simulations. Such autoresonantly excited multiphase waves form coherent quasicrystalline structures, which can potentially be used as plasma photonic or accelerating devices. Finally, we discuss the laser parameters required for the autoresonant excitation of nonlinear waves in a plasma.

I. INTRODUCTION

The electron plasma wave is perhaps the most studied collective oscillation in a plasma, yet the nonlinear behavior of the electron plasma wave, including fluid and kinetic effects, remains an active topic of research [1–16] even after decades of study. Nonlinear effects in electron plasma waves are important for many applications of laser-plasma interactions, including ultra-high gradient accelerators [17], inertial confinement fusion (ICF) [18], and photonics for extremely intense laser pulses [19].

In most applications, the electron plasma wave is controlled by the ponderomotive force of one or more lasers. For example, in plasma photonics, complex density structures are envisioned for transient plasma gratings [20], holographic gratings [21], and polarizers [22–25]. Resonant plasma instabilities, and the concomitant density modulations, lead to energy transfer between laser pulses. In the Raman backscatter amplifier, energy in a long laser pulse is transferred to a counter-propagating short pulse [26]. Crossbeam energy transfer [27] makes use of a resonance with an ion acoustic wave and is routinely utilized to control asymmetries in target illumination at the National Ignition Facility (NIF).

Autoresonance is a phenomenon of nonlinear science that has ample applications in plasma, astro-, and atomic physics [28, 29]. The basic idea of autoresonance lies in the ability of a nonlinear system to remain in resonance by phase locking (synchronization) with external drives with adiabatically varying parameters. It has been proposed as a method to create a large amplitude traveling plasma wave using two co-propagating lasers with a chirped frequency mismatch [30] that passes through the linear electron plasma wave frequency. In spatial autoresonance, two constant frequency lasers propagate parallel to a plasma density gradient [31] with the linear resonance at a specific location in the plasma. In autoresonance, the nonlinear oscillator maintains synchronism with a chirped-frequency drive so long as a threshold condition, which relates the chirp rate to the drive amplitude, is satisfied. Autoresonance can be used as a method to excite large amplitude traveling ion acoustic waves [32, 33].

Autoresonant excitation of electron plasma and ion acoustic waves is not limited to traveling waves. It was shown in Ref. [34] that a large amplitude standing ion acoustic wave can be formed using two counter-propagating ponderomotive drives with a chirped frequency difference. This standing wave comprises a particular nonlinear two-phase ion acoustic wave structure, wherein each locked phase corresponds to one of the counter-propagating traveling drives. Large amplitude standing electron plasma waves can be created with autoresonant drives [35].

It has been shown, using both theory and numerical simulations, that one can use autoresonance to construct multiphase solutions for integrable systems, such as the Korteweg–de Vries (KdV) equation [36], the Toda lattice [37], the nonlinear Schrödinger equation [38], and the sine-Gordon equation [39]. Multiphase nonlinear waves are significantly more difficult to analyze theoretically than traveling waves, which can be described by a single phase. The theory for autoresonant wave excitation, nevertheless, has been extended to two-phase nonlinear waves. In a recent publication [40], we demonstrated how autoresonance can be used to create two-phase solutions in the generally non-integrable system of equations describing ion acoustic waves. This extends the earlier work where the autoresonant excitation was analyzed for nonlinear single phase [32, 33] and standing [34] ion acoustic waves. In Ref. [35], it was shown that autoresonance can be used to excite large amplitude standing electron plasma waves, which can be regarded as a particular case of a more general two-phase solution. In this paper we will show that the system describing plasma waves indeed exhibits nonlinear two-phase solutions that are characteristic of integrable partial differential equations. Similar to the case of ion acoustic waves [40], space-time qua-

* vmunirov@berkeley.edu

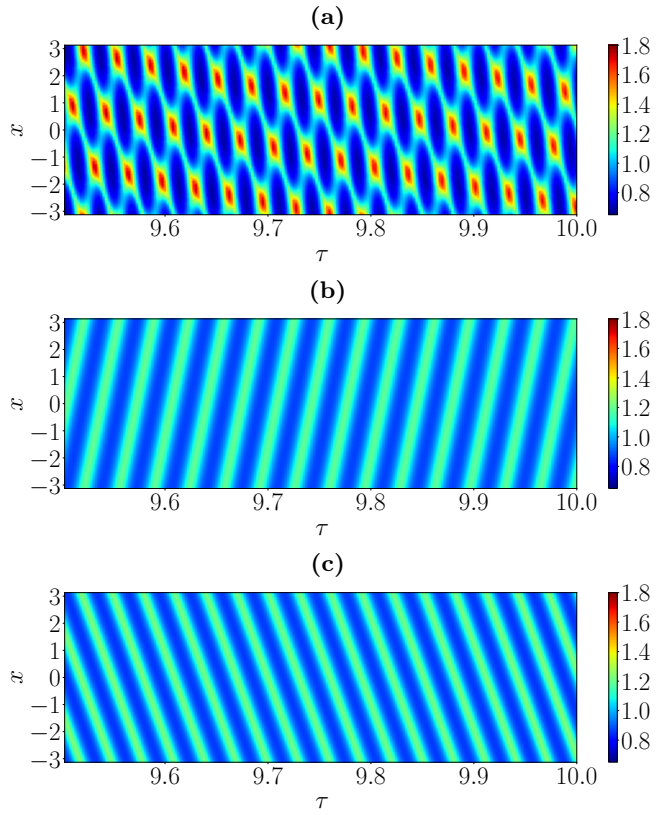

FIG. 1. The colormap of the electron density $n_e(x,\tau)$ as a function of slow time $\tau = \sqrt{\alpha_1}t$ and coordinate x obtained by solving the fully nonlinear equations (1)–(3). (a) Two-phase autoresonant plasma wave excited by two driving counter-propagating traveling waves with $k_1 = 1$ and $k_2 = -2$. (b) Single phase autoresonant plasma wave excited solely by the first driving component with $k_1 = 1$. (c) Single phase autoresonant plasma wave excited solely by the second driving component with $k_2 = -2$.

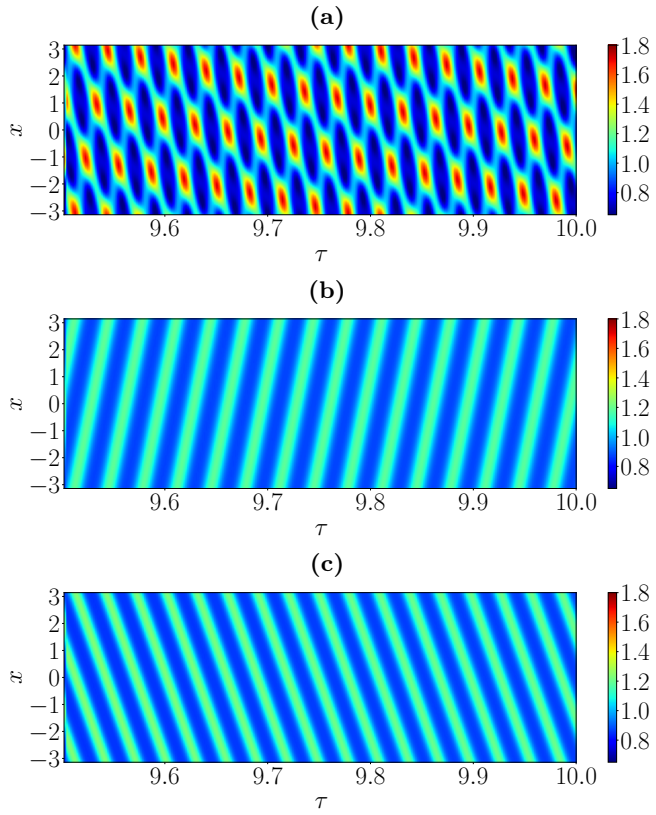

FIG. 2. The colormap of the electron density $n_e(x,\tau)$ as a function of slow time $\tau = \sqrt{\alpha_1}t$ and coordinate x obtained by solving the weakly nonlinear equations (32)–(35). (a) Two-phase autoresonant plasma wave excited by two driving counter-propagating traveling waves with $k_1 = 1$ and $k_2 = -2$. (b) Single phase autoresonant plasma wave excited solely by the first driving component with $k_1 = 1$. (c) Single phase autoresonant plasma wave excited solely by the second driving component with $k_2 = -2$.

sicrystalline structures formed by the autoresonantly excited multiphase nonlinear plasma waves can potentially be used as plasma photonic or, perhaps, even, as specialized accelerating structures.

This paper is organized as follows. In Sec. II, we present a warm fluid model of partial differential equations describing electron plasma waves, and we demonstrate, through fully nonlinear numerical simulations, that it supports a two-phase solution. In Sec. III, we apply Whitham's averaged variational principle [41, 42] to the Lagrangian formulation of the fluid equations and develop an analytical weakly nonlinear theory in the form of a system of coupled ordinary differential equations; this system is shown to yield a good approximation of the fully nonlinear model. In Sec. IV, we estimate the laser pulse intensity and duration required for autoresonant excitation of nonlinear plasma and ion acoustic waves. Finally, a summary and concluding remarks are given in Sec. V.

II. NUMERICAL STUDY OF THE EXCITATION OF MULTIPHASE NONLINEAR PLASMA WAVES

A warm fluid model of electron plasma waves is constituted by a system of continuity, momentum, and Poisson's equations:

$$\sigma_{xt} + \left[\left(1+\sigma_x\right)\psi_x\right]_x = 0, \tag{1}$$

$$\psi_{xt} + \psi_x\psi_{xx} = \left(\varphi+\varphi_d\right)_x - \Delta^2\left(1+\sigma_x\right)\sigma_{xx}, \tag{2}$$

$$\varphi_{xx} = \kappa^2\varphi + \sigma_x. \tag{3}$$

Here we introduced potentials σ and ψ, which are defined through $n_e = 1+\sigma_x$, $v = \psi_x$, where n_e is the electron density and v is the fluid velocity. Other variables are the electric potential φ and the driving potential φ_d. Parameter κ is the effective screening parameter (see Refs. [12, 35]), while $\Delta^2 = 3u_{th}^2$, where u_{th} is the electron thermal velocity which is assumed constant.

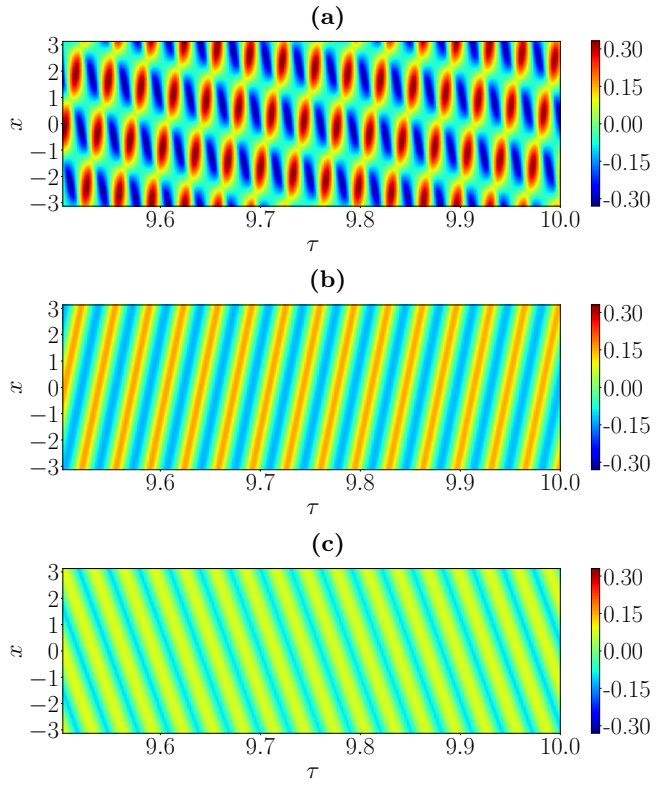

FIG. 3. The colormap of the electron fluid velocity $v(x,\tau)$ as a function of slow time $\tau = \sqrt{\alpha_1}t$ and coordinate x obtained by solving the fully nonlinear equations (1)–(3). (a) Two-phase autoresonant plasma wave excited by two driving counter-propagating traveling waves with $k_1 = 1$ and $k_2 = -2$. (b) Single phase autoresonant plasma wave excited solely by the first driving component with $k_1 = 1$. (c) Single phase autoresonant plasma wave excited solely by the second driving component with $k_2 = -2$.

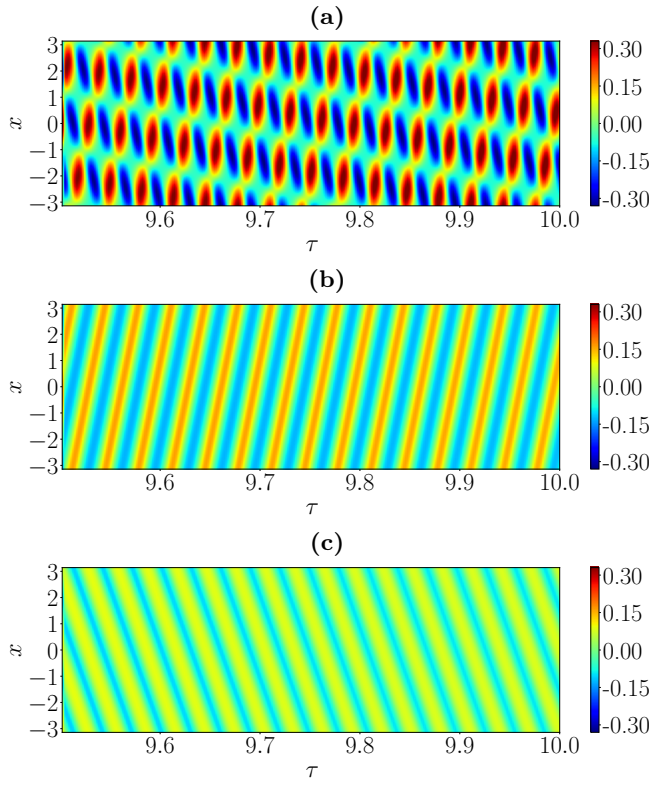

FIG. 4. The colormap of the electron fluid velocity $v(x,\tau)$ as a function of slow time $\tau = \sqrt{\alpha_1}t$ and coordinate x obtained by solving the weakly nonlinear equations (32)–(35). (a) Two-phase autoresonant plasma wave excited by two driving counter-propagating traveling waves with $k_1 = 1$ and $k_2 = -2$. (b) Single phase autoresonant plasma wave excited solely by the first driving component with $k_1 = 1$. (c) Single phase autoresonant plasma wave excited solely by the second driving component with $k_2 = -2$.

All variables are dimensionless; specifically, the time is measured in terms of the inverse plasma frequency ω_p^{-1}, the distance is normalized to k^{-1}, where k is the typical wave vector, the plasma density is normalized to the unperturbed plasma density, and the electric and driving potentials are normalized to $m_e\omega_p^2/ek^2$.

We consider the driving term consisting of the two small amplitude traveling wave ponderomotive drives:

$$\varphi_d = \varepsilon_1 \cos(\theta_{d,1}) + \varepsilon_2 \cos(\theta_{d,2}), \tag{4}$$

where $\theta_{d,i} = k_i x - \int \omega_{d,i}(t)\,dt$ $(i = 1,2)$ are driving phases with wave vectors k_i and slowly varying driving frequencies $\omega_{d,i}(t) = -d\theta_{d,i}/dt$.

To illustrate autoresonant excitation of single and multiphase plasma waves, let us consider a representative example of two driving counter-propagating traveling waves with wave vectors $k_1 = 1$ and $k_2 = -2$. We choose their chirped driving frequencies as

$$\omega_{d,i} = \begin{cases} \omega_{p,i} + \alpha_i t, & t \le 0, \\ \omega_{p,i} + \alpha_i T_i \arctan\left(\frac{t}{T_i}\right), & t > 0, \end{cases} \tag{5}$$

where $T_i = 2\Delta\omega_i/\pi\alpha_i$ $(i = 1,2)$, $\alpha_1 = \alpha_2 = 2.5\times10^{-5}$, $\Delta\omega_1 = \Delta\omega_2 = 0.008$ and $\omega_{p,i}$ $(i = 1,2)$ are the frequencies given by the linear plasma wave dispersion relation:

$$\omega_{p,i}(k_i) = \sqrt{\frac{1}{1+\frac{\kappa^2}{k_i^2}} + \Delta^2 k_i^2}. \tag{6}$$

We also gradually increase the driving amplitudes as $\varepsilon_i = \bar{\varepsilon}_i\left[0.5 + \arctan\left(t\sqrt{\alpha_i}/10\right)/\pi\right]$, $\bar{\varepsilon}_i = 2\times10^{-3}$ $(i = 1,2)$. We take the electron thermal velocity and the effective screening parameter to be $u_{th} = 0.1$ and $\kappa = 0.5$, respectively. We use the wave vector of the first drive k_1 as the typical wave vector k (hence, $k_1 = 1$).

The system of nonlinear partial differential equations (1)–(3) can be solved numerically. To do this we

use a pseudospectral method [43] in space and the fourth-order Runge–Kutta method for the time advancement, similar to the procedure employed in Refs. [33–35, 40]. We run simulations from $\tau = -10$ and stop the driving at $\tau = 10$, where $\tau = \sqrt{\alpha_1}t$ is a slow time variable. The results of the fully nonlinear numerical simulations with the parameters specified above are presented in Figs. 1, 3, and 5.

Figure 1 shows a colormap of the electron density $n_e(x,\tau)$ as a function of slow time τ and coordinate x for τ between $\tau = 9.5$ and $\tau = 10$. Figure 1(a) shows a two-phase nonlinear electron plasma wave excited by two small amplitude chirped-frequency traveling waves with $k_1 = 1$ and $k_2 = -2$. Figure 1(b) shows a single phase plasma wave autoresonantly excited only by the first chirped-frequency traveling wave drive with $k_1 = 1$, using the same parameters in the drive as in Fig. 1(a) but with vanishing ε_2, while Fig. 1(c) shows a single phase plasma wave autoresonantly excited by the chirped-frequency traveling wave drive with $k_2 = -2$, using the same parameters in the drive as in Fig. 1(a) but with vanishing ε_1. Figure 3 is identical to Fig. 1 but shows a colormap of the fluid velocity $v(x,\tau)$ as a function of slow time τ and coordinate x instead. We can clearly see from Figs. 1 and 3 that a highly nonlinear large amplitude ($\delta n_e/n_e \sim 1$) two-phase, quasiperiodic in space and time, structure is excited by the drives. We can also see that the directions of the phase velocities of the single phase waves [see Figs. 1(b) and 1(c)] correspond to the characteristic directions seen in the two-phase solution [see Fig. 1(a)]. We also note that, as in the case of ion acoustic waves [40], the nonlinear structures persist even after we turn off the small amplitude drives (not shown in the figures).

Figure 5 shows the maximum value over x of the electron density $n_e(x,\tau)$ [Fig. 5(a)] and of the fluid velocity $v(x,\tau)$ [Fig. 5(b)] versus slow time $\tau = \sqrt{\alpha_1}t$ from the start of the simulation at $\tau = -10$ to $\tau = 10$. We can see that the system passes the linear plasma resonance at $\tau = 0$ and then the amplitudes of both waves rapidly increase, reaching large values. This happens because, due to nonlinear effects, the waves alter their amplitudes in a way that lets them stay phase-locked with the external drives, allowing the continuous transfer of energy from the drives to the excitations.

To better understand the nature of the double autoresonance, and to have a tool to select the appropriate parameters required to establish the autoresonance, we need to develop a theory. To that end, in the next section, we will formulate the problem in the Lagrangian language and then use Whitham's averaged variational principle [41, 42] to obtain the simplified weakly nonlinear equations describing the evolution of the system.

III. WEAKLY NONLINEAR THEORY AND WHITHAM'S VARIATIONAL METHOD

The system of nonlinear equations (1)–(3) can be described using the Lagrangian formalism. Indeed, one can check that Eqs. (1)–(3) are, in fact, the Euler–Lagrange equations of the form

$$\frac{\partial L}{\partial \sigma} - \frac{\partial}{\partial t}\frac{\partial L}{\partial \sigma_t} - \frac{\partial}{\partial x}\frac{\partial L}{\partial \sigma_x} = 0, \tag{7}$$

$$\frac{\partial L}{\partial \psi} - \frac{\partial}{\partial t}\frac{\partial L}{\partial \psi_t} - \frac{\partial}{\partial x}\frac{\partial L}{\partial \psi_x} = 0, \tag{8}$$

$$\frac{\partial L}{\partial \varphi} - \frac{\partial}{\partial t}\frac{\partial L}{\partial \varphi_t} - \frac{\partial}{\partial x}\frac{\partial L}{\partial \varphi_x} = 0, \tag{9}$$

which emerge from the following Lagrangian density:

$$L = \frac{1}{2}\varphi_x^2 + \frac{1}{2}\kappa^2\varphi^2 - \frac{1}{2}(\psi_t\sigma_x + \psi_x\sigma_t) - \frac{1}{2}\psi_x^2(1+\sigma_x) - \frac{1}{2}\Delta^2\sigma_x^2\left(1+\frac{1}{3}\sigma_x\right) + \sigma_x(\varphi+\varphi_d). \tag{10}$$

Since we use slowly varying driving frequencies, it is appropriate to exploit a natural separation into slow and fast dynamics. We now proceed to derive equations describing the slow evolution of the waves in space and time. Whitham [41, 42] demonstrated how to obtain such equations on the basis of the Lagrangian formalism. In this section, we will employ Whitham's averaged Lagrangian method to obtain weakly nonlinear equations describing the evolution of the slow variables. We will closely follow the procedure that we used to study multiphase ion acoustic waves described in Ref. [40].

Let us first examine the linear stage of the evolution. If we start from the equilibrium solution ($n_e = 1$, $v = 0$, $\varphi = 0$), then it is straightforward to show that during the linear stage the solutions are given by

$$\sigma = \tilde{A}_{10}\sin(\theta_1) + \tilde{A}_{01}\sin(\theta_2), \tag{11}$$

$$\psi = \tilde{B}_{10}\sin(\theta_1) + \tilde{B}_{01}\sin(\theta_2), \tag{12}$$

$$\varphi = C_{10}\cos(\theta_1) + C_{01}\cos(\theta_2), \tag{13}$$

where the linear amplitudes satisfy

$$C_{10} = \frac{\varepsilon_1}{(\omega_1^2 - \Delta^2 k_1^2)\left(1+\frac{\kappa^2}{k_1^2}\right) - 1}, \tag{14}$$

$$C_{01} = \frac{\varepsilon_2}{(\omega_2^2 - \Delta^2 k_2^2)\left(1+\frac{\kappa^2}{k_2^2}\right) - 1}, \tag{15}$$

$$\tilde{A}_{10} = -k_1\left(1+\frac{\kappa^2}{k_1^2}\right)C_{10}, \tag{16}$$

$$\tilde{A}_{01} = -k_2\left(1+\frac{\kappa^2}{k_2^2}\right)C_{01}, \tag{17}$$

$$\tilde{B}_{10} = -\omega_1 \left(1 + \frac{\kappa^2}{k_1^2}\right) C_{10}, \tag{18}$$

$$\tilde{B}_{01} = -\omega_2 \left(1 + \frac{\kappa^2}{k_2^2}\right) C_{01}. \tag{19}$$

The form of the driving potential together with the linear stage solution suggest using the following weakly nonlinear ansatz describing the two-phase solutions for the potentials σ, ψ, and φ:

$$\begin{aligned}\sigma = {} & \tilde{A}_{10} \sin(\theta_1) + \tilde{A}_{01} \sin(\theta_2) \\ & + \tilde{A}_{11} \sin(\theta_1 + \theta_2) + \tilde{A}_{1,-1} \sin(\theta_1 - \theta_2) \\ & + \tilde{A}_{20} \sin(2\theta_1) + \tilde{A}_{02} \sin(2\theta_2), \end{aligned} \tag{20}$$

$$\begin{aligned}\psi = {} & \tilde{B}_{10} \sin(\theta_1) + \tilde{B}_{01} \sin(\theta_2) \\ & + \tilde{B}_{11} \sin(\theta_1 + \theta_2) + \tilde{B}_{1,-1} \sin(\theta_1 - \theta_2) \\ & + \tilde{B}_{20} \sin(2\theta_1) + \tilde{B}_{02} \sin(2\theta_2), \end{aligned} \tag{21}$$

$$\begin{aligned}\varphi = {} & C_{10} \cos(\theta_1) + C_{01} \cos(\theta_2) \\ & + C_{11} \cos(\theta_1 + \theta_2) + C_{1,-1} \cos(\theta_1 - \theta_2) \\ & + C_{20} \cos(2\theta_1) + C_{02} \cos(2\theta_2), \end{aligned} \tag{22}$$

where $\theta_i = k_i x - \int \omega_i(t)\, dt$ $(i = 1, 2)$ are phases of the solutions.

Note that the above solutions correspond not to the superposition of two separate nonlinear waves as in Ref. [44], but to a single two-phase nonlinear wave, i.e., the solutions have the form $f(\theta_1, \theta_2)$ as opposed to $f(\theta_1, \theta_2) = f_1(\theta_2) + f_2(\theta_2)$.

To explicitly separate slow and fast phase variables we introduce phase mismatches $\Phi_i = \theta_i - \theta_{d,i}$ $(i = 1, 2)$ between phases of the solutions θ_i and the driving phases $\theta_{d,i}$, so that the driving term given by Eq. (4) becomes $\varphi_d = \varepsilon_1 \cos(\theta_1 - \Phi_1) + \varepsilon_2 \cos(\theta_2 - \Phi_2)$. It should be understood then that the coefficients in our ansatz and phase mismatches Φ_1, Φ_2 are slow functions of time, while the phases θ_1, θ_2 are rapidly varying functions of time.

According to Whitham's variational principle, we need to obtain the averaged Lagrangian density $\bar{L}$ by integrating the full Lagrangian density (10) over the rapidly varying phases θ_1, θ_2:

$$\bar{L} = \langle L \rangle_{\theta_1, \theta_2} = \int L \frac{d\theta_1}{2\pi} \frac{d\theta_2}{2\pi}. \tag{23}$$

The resulting averaged Lagrangian density $\bar{L}$ will be a function of the slowly varying amplitudes and the phase mismatches only. This averaged Lagrangian is presented in Appendix A.

After obtaining the averaged Lagrangian density $\bar{L}$, we can use the variational principle $\delta\left(\int \bar{L} dx dt\right) = 0$ to derive the weakly nonlinear equations that describe the evolution of slowly modulated parameters (amplitudes and phase mismatches).

Following Ref. [40], we first take variations with respect to the phases and, after keeping the lowest significant order terms and using the linear relations (16)–(19), we obtain

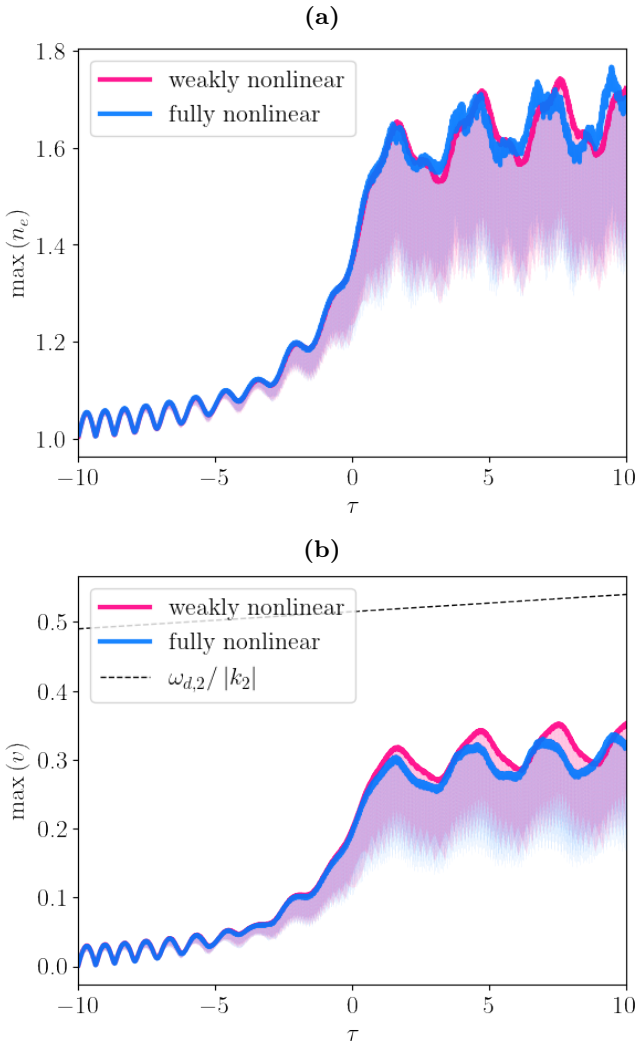

FIG. 5. The maximum over x of the electron density $n_e(x, \tau)$ (a) and the electron fluid velocity $v(x, \tau)$ (b) versus slow time $\tau = \sqrt{\alpha_1} t$ for a two-phase autoresonant ion acoustic wave excited by two driving counter-propagating traveling waves with $k_1 = 1$ and $k_2 = -2$. The solutions were obtained by solving the fully nonlinear equations (1)–(3) (denoted as "fully nonlinear", blue line) and the weakly nonlinear equations (32)–(35) (denoted as "weakly nonlinear", pink line). The dashed black line represents the absolute value of the phase velocity of the second driving wave $\omega_{d,2}(\tau)/|k_2|$ versus τ.

$$\frac{d}{dt}\left[\omega_1\left(1+\frac{\kappa^2}{k_1^2}\right)C_{10}^2\right] = -\varepsilon_1 C_{10}\sin\left(\Phi_1\right), \tag{24}$$

$$\frac{d}{dt}\left[\omega_2\left(1+\frac{\kappa^2}{k_2^2}\right)C_{01}^2\right] = -\varepsilon_2 C_{01}\sin\left(\Phi_2\right). \tag{25}$$

Taking variations of the averaged Lagrangian density $\bar{L}$ with respect to the first-order amplitudes and expanding around the linear dispersion relation $\omega_i = \omega_{p,i} + \Delta\omega_i$ $(i = 1, 2)$, we obtain

$$\begin{aligned}\Delta\omega_1 = &-2\omega_1 k_1^2\left(1+\frac{\kappa^2}{k_1^2}\right)^2 a\left(k_1,\omega_1\right)C_{10}^2 \\ &- 2\omega_2 k_2^2\left(1+\frac{\kappa^2}{k_2^2}\right)^2 b\left(k_1,\omega_1;k_2,\omega_2\right)C_{01}^2 \\ &+ \frac{\varepsilon_1}{2\omega_1\left(1+\frac{\kappa^2}{k_1^2}\right)C_{10}}\cos\left(\Phi_1\right),\end{aligned} \tag{26}$$

$$\begin{aligned}\Delta\omega_2 = &-2\omega_2 k_2^2\left(1+\frac{\kappa^2}{k_2^2}\right)^2 c\left(k_2,\omega_2\right)C_{01}^2 \\ &- 2\omega_1 k_1^2\left(1+\frac{\kappa^2}{k_1^2}\right)^2 b\left(k_1,\omega_1;k_2,\omega_2\right)C_{10}^2 \\ &+ \frac{\varepsilon_2}{2\omega_2\left(1+\frac{\kappa^2}{k_2^2}\right)C_{01}}\cos\left(\Phi_2\right),\end{aligned} \tag{27}$$

where the functions $a\left(k_1,\omega_1\right)$, $b\left(k_1,\omega_1;k_2,\omega_2\right)$, $c\left(k_2,\omega_2\right)$ are defined in Appendix B.

Notice that for $\varepsilon_1 = \varepsilon_2 = 0$, $C_{01} = 0$, and $\kappa = 0$, we obtain from Eqs. (26)–(27) the nonlinear frequency shift for a single nonlinear wave in the absence of the drives:

$$\frac{\Delta\omega_1}{\omega_1} = k_1^4\frac{6+9\frac{\Delta^2 k_1^2}{\omega_1^2}+\left(\frac{\Delta^2 k_1^2}{\omega_1^2}\right)^2}{12\left(1-\frac{\Delta^2 k_1^2}{\omega_1^2}\right)}C_{10}^2, \tag{28}$$

which agrees with the nonlinear frequency shift for a single nonlinear wave in the lab frame (see Ref. [13] and references therein).

Finally, assuming a slow drive of the form $\omega_{d,i}\left(t\right) = \omega_{p,i} + f_i\left(t\right)$ and defining the effective action variables and rescaled amplitudes through

$$I_1 = 2\omega_1 k_1^2\left(1+\frac{\kappa^2}{k_1^2}\right)^2 C_{10}^2, \tag{29}$$

$$I_2 = 2\omega_2 k_2^2\left(1+\frac{\kappa^2}{k_2^2}\right)^2 C_{01}^2, \tag{30}$$

$$\epsilon_1 = -2\left|k_1\right|\varepsilon_1,\ \epsilon_2 = -2\left|k_2\right|\varepsilon_2, \tag{31}$$

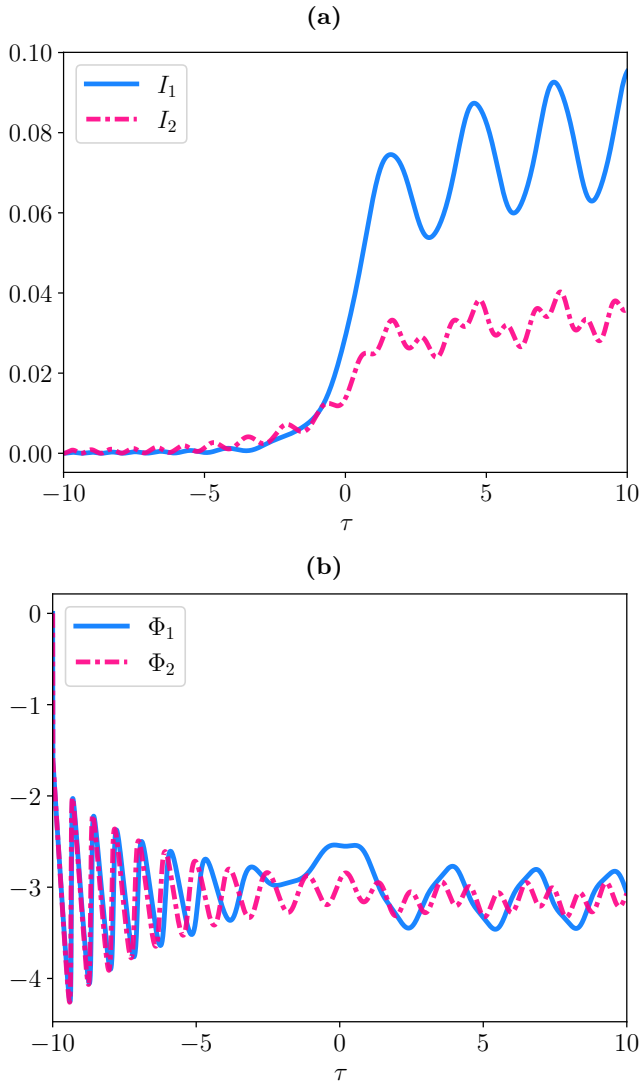

FIG. 6. The effective actions I_1, I_2 (a) and the phase mismatches Φ_1, Φ_2 (b) as functions of slow time $\tau = \sqrt{\alpha_1}t$ obtained by solving the weakly nonlinear equations (32)–(35).

we can rewrite Eqs. (24)–(27) and obtain the following system of coupled weakly nonlinear evolution equations:

$$\frac{dI_1}{dt} = \epsilon_1\sqrt{\frac{I_1}{2\omega_1}}\sin\left(\Phi_1\right), \tag{32}$$

$$\frac{dI_2}{dt} = \epsilon_2\sqrt{\frac{I_2}{2\omega_2}}\sin\left(\Phi_2\right), \tag{33}$$

$$\frac{d\Phi_1}{dt} = aI_1 + bI_2 + f_1\left(t\right) + \frac{\epsilon_1}{2\sqrt{2\omega_1 I_1}}\cos\left(\Phi_1\right), \tag{34}$$

$$\frac{d\Phi_2}{dt} = bI_1 + cI_2 + f_2\left(t\right) + \frac{\epsilon_2}{2\sqrt{2\omega_2 I_2}}\cos\left(\Phi_2\right). \tag{35}$$

The coupled weakly nonlinear equations (32)–(35) comprise a system of ordinary differential equations and can be easily solved using any modern numerical li-

brary. Thus, the system of the weakly nonlinear equations (32)–(35) allows us to obtain straightforward numerical solutions as well as to study the conditions for double autoresonance. The possibility of exciting double autoresonance and limitations on the parameter space in the systems governed by Eqs. (32)–(35) were discussed in detail in Ref. [40] (see also Ref. [45]), so we will not repeat them here. These results can be easily reproduced for the functional forms of $a\left(k_1,\omega_1\right)$, $b\left(k_1,\omega_1;k_2,\omega_2\right)$, $c\left(k_2,\omega_2\right)$ given in Appendix B.

The results of the numerical solution of the weakly nonlinear system (32)–(35) are presented in Figs. 2, 4–6. The parameters used in the simulations are identical to the ones used in the fully nonlinear numerical simulations of the previous section. Figure 2 shows a colormap of the electron density $n_e\left(x,\tau\right)$ versus slow time τ and coordinate x (as in Fig. 1), while Fig. 4 shows a similar colormap but for the fluid velocity $v\left(x,\tau\right)$ (as in Fig. 3). After comparing Fig. 1 with Fig. 2 and Fig. 3 with Fig. 4, we can conclude that the weakly nonlinear theory works well in modeling the original system. This should be even clearer from Fig. 5, which compares the maximum values over x of the electron densities $n_e\left(x,\tau\right)$ [Fig. 5(a)] and of the fluid velocities $v\left(x,\tau\right)$ [Fig. 5(b)] in the original fully nonlinear simulations (blue color) and in the weakly nonlinear model (pink color). Indeed, despite a high degree of nonlinearity, the agreement is quite decent. Figure 5(b) also shows the absolute value of the phase velocity of the second driving wave with $k_2=-2$. We can see that the fluid velocity is below the absolute values of the phase velocities of the driving waves, which means we are below the wave breaking limit for the parameters chosen.

Figure 6 shows the effective actions I_1, I_2 [Fig. 6(a)] and the phase mismatches Φ_1, Φ_2 [Fig. 6(b)] versus slow time $\tau=\sqrt{\alpha_1}t$. We can clearly see that the phase mismatches oscillate around $-\pi$, signifying phase locking, while the effective actions I_1, I_2 enter the resonance at $\tau=0$ and then remain in the resonance and grow rapidly.

It is known that the autoresonant phenomenon occurs only when the driving amplitudes exceed certain threshold values; see Refs. [40, 45]. The threshold nature of the autoresonance manifests itself for the system described in this paper as well. As was discussed in Ref. [40], it is difficult to obtain the general analytical result for the double autoresonance thresholds for the systems described by Eqs. (32)–(35), and the thresholds are complicated functions of α_1, α_2, a, b, c. However, the threshold condition for a single phase wave, i.e., when one of the driving amplitudes in Eqs. (32)–(35) vanishes, is well known [37]:

$$\left|\epsilon_1\right|>1.644\sqrt{\frac{\omega_1}{2\left|a\left(k_1,\omega_1\right)\right|}}\alpha^{\frac{3}{4}}, \tag{36}$$

where we assumed the presence of the first drive only ($\epsilon_2=0$) and the linear chirp rate α.

In the next section, we will use the threshold condition (36) to estimate the experimental parameters, such as laser intensity and laser pulse length required for the autoresonant excitation of plasma and ion acoustic waves.

IV. ESTIMATES OF LASER PARAMETERS

In this section we estimate the required laser pulse intensity and length necessary for autoresonant excitation of large amplitude waves. We will make estimates of the autoresonant excitation of both plasma waves discussed in this paper and of ion acoustic waves studied in Ref. [40]. Since the threshold conditions for double autoresonance are difficult to obtain in generality, we will consider autoresonant excitation of single phase waves here. Nevertheless, as indicated by numerical simulations, the single phase estimates should be good proxies for multiphase waves as well.

A. Ion acoustic waves

First, let us consider the case of ion acoustic waves discussed in Ref. [40]. In this subsection, all the variables are as they are defined in Ref. [40].

The ponderomotive drive can be created by launching two co- or counter-propagating laser pulses of similar intensity and duration with varying (chirped) frequencies; the associated beat wave will produce the ponderomotive potential with the required properties.

From the single phase threshold condition [Eq. (36)], using definitions of the dimensionless quantities from Ref. [40], we find the following approximate condition for the autoresonance in the system of ion acoustic waves:

$$\mathrm{LHS}\left(I,\lambda,n_e/n_c,T_e\right)>\mathrm{RHS}\left(k_1,\alpha\right), \tag{37}$$

where we introduced the functions

$$\mathrm{LHS}\left(I,\lambda,n_e/n_c,T_e\right)=\frac{U_p\left[\mathrm{eV}\right]}{T_e\left[\mathrm{eV}\right]}, \tag{38}$$

$$\mathrm{RHS}\left(k_1,\alpha\right)=1.644\sqrt{\frac{\omega_1}{2\left|a\left(k_1,\omega_1\right)\right|}}\frac{\left|k_1\right|}{2\left(\omega_1^2-\Delta^2k_1^2\right)}\alpha^{\frac{3}{4}}. \tag{39}$$

Here, T_e is the initial electron temperature and U_p is the ponderomotive energy given by

$$U_p\left[\mathrm{eV}\right]=9.33\times10^{-14}I\left[\frac{\mathrm{W}}{\mathrm{cm}^2}\right]\lambda^2\left[\mu\mathrm{m}\right]\sqrt{1-\frac{n_e}{n_c}}, \tag{40}$$

where I is the laser intensity, λ is the laser wavelength, and n_e/n_c is the ratio of the initial electron density to the critical plasma density. Inside the function $\mathrm{RHS}\left(k_1,\alpha\right)$ [Eq. (39)] we have the dimensionless wave vector k_1 (measured in units of the inverse Debye length λ_D^{-1}) and the

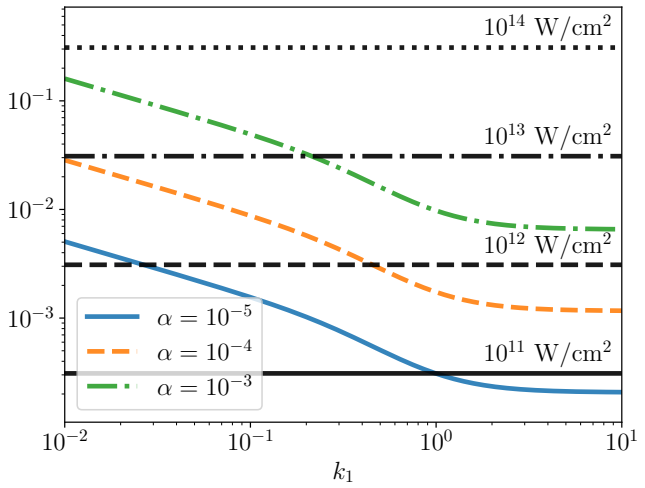

FIG. 7. Approximate thresholds for autoresonant excitation of single phase ion acoustic waves. The figure shows the LHS $\left(I, \lambda = 1\ \mu\text{m}, n_e/n_c = 10^{-2}, T_e = 30\ \text{eV}\right)$ given by Eq. (38) for different values of the laser intensity I [$I = 10^{11}$ W/cm^2 (solid black), $I = 10^{12}$ W/cm^2 (dashed black), $I = 10^{13}$ W/cm^2 (dash-dotted black), and $I = 10^{14}$ W/cm^2 (dotted black)] and the RHS (k_1, α) given by Eq. (39) for different values of chirp rate α [$\alpha = 10^{-5}$ (solid blue), $\alpha = 10^{-4}$ (dashed orange), and $\alpha = 10^{-3}$ (dash-dotted green)] as functions of k_1. For the autoresonance to occur, the RHS must be below the horizontal line representing the LHS.

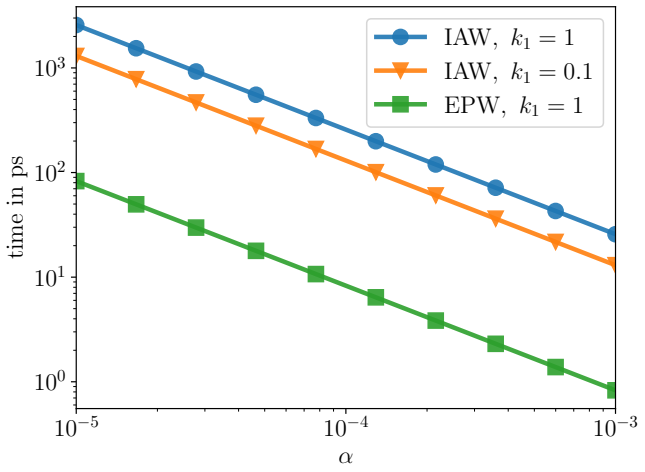

FIG. 8. Estimate of the laser pulse length required for the autoresonant excitation of nonlinear waves. The figure shows t_{pulse} given by Eq. (41) in picoseconds required for $(\delta n_e/n_e)_1$ to reach 0.25 in autoresonant excitation of ion acoustic waves (IAW) for $k_1 = 0.1$ (orange line with triangle markers) and $k_1 = 1$ (blue line with circle markers) as functions of chirp rate α. In addition, the figure shows t_{pulse} given by Eq. (44) in picoseconds required for $(\delta n_e/n_e)_1$ to reach 0.25 in autoresonant excitation of electron plasma waves (EPW) for $k_1 = 1$ (green line with square markers) as a function of chirp rate α.

dimensionless frequency ω_1 (measured in units of the ion plasma frequency ω_{pi}) given by the linear ion acoustic wave dispersion relation (see Ref. [40]); the definitions of $a\left(k_1, \omega_1\right)$, ω_1, k_1, Δ, and α are from Ref. [40].

Figure 7 shows the LHS given by Eq. (38) for different values of the laser intensity I and the RHS given by Eq. (39) for different values of chirp rate α as functions of dimensionless k_1 (measured in λ_D^{-1}) for $\lambda = 1\ \mu$m, $n_e/n_c = 10^{-2}$, $T_e = 30$ eV, and cold ions ($\Delta = 0$). For the autoresonance to occur, the RHS for given values of α and k_1 must be below the horizontal line representing the LHS for a given value of I.

We note that one must take into account additional physical restrictions on the accessible values of k_1. For example, to avoid strong Landau damping, k_1 cannot be too large. We now estimate the required laser intensity for two realistic values of the dimensionless wave vector $k_1 = 0.1$ and $k_1 = 1$. We see from Fig. 7 that for the chosen parameters, if $k_1 = 0.1$, autoresonance occurs when the laser intensity exceeds $I \approx 10^{14}$ W/cm^2 for $\alpha = 10^{-3}$, $I \approx 10^{13}$ W/cm^2 for $\alpha = 10^{-4}$, and $I \approx 10^{12}$ W/cm^2 for $\alpha = 10^{-5}$, while if $k_1 = 1$, the intensity should exceed $I \approx 10^{13}$ W/cm^2 for $\alpha = 10^{-3}$, $I \approx 10^{12}$ W/cm^2 for $\alpha = 10^{-4}$, and $I \approx 10^{11}$ W/cm^2 for $\alpha = 10^{-5}$.

Now let us estimate the laser duration required to autoresonantly excite large amplitude waves. Since the electron density in Ref. [40] can be approximated as e^{φ}, we can estimate in the leading linear order the relative density increase as $(\delta n_e)_1 \approx (\delta\varphi)_1 \approx C_{10}$. Then, using the asymptotic solution for the effective action $\bar{I}_1 \approx \left[\alpha/\left|a\left(k_1, \omega_1\right)\right|\right] t$ and its connection with C_{10} (see definitions of Ref. [40]), we can estimate the dimensionless laser pulse length (measured in units of ω_{pi}^{-1}) required to reach $(\delta n_e/n_e)_1$ as

$$t_{\text{pulse}} = \left[\left(\frac{\delta n_e}{n_e}\right)_1\right]^2 \frac{2\omega_1 k_1^2}{\left(\omega_1^2 - \Delta^2 k_1^2\right)^2} \frac{\left|a\left(k_1, \omega_1\right)\right|}{\alpha}, \qquad (41)$$

where the definitions of $a\left(k_1, \omega_1\right)$, ω_1, k_1, Δ, and α are from Ref. [40].

Figure 8 plots the pulse length determined by Eq. (41) in picoseconds as a function of chirp rate α for $(\delta n_e/n_e)_1 = 0.25$ for $k_1 = 0.1$ (orange line with triangle markers) and $k_1 = 1$ (blue line with circle markers). Other parameters are the same as in Fig. 7, namely $\lambda = 1\ \mu$m, $n_e/n_c = 10^{-2}$, $T_e = 30$ eV, $\Delta = 0$. We can see that for $\alpha = 10^{-4}$ the laser pulse length of $t_{\text{pulse}} \approx 10$–$100$ ps is required, while for $\alpha = 10^{-3}$ the laser pulse length of $t_{\text{pulse}} \approx 1$–$10$ ps should be sufficient.

We note that the chosen linear increase in the relative density $(\delta n_e/n_e)_1 = 0.25$ corresponds in practice to large density fluctuations on the order of $\delta n_e/n_e \sim 1$. We also note that even though for the two-phase case there are additional restrictions on the values of ε_1, ε_2, α_1, α_2, k_1, and k_2, the actual requirements for the laser intensity and duration can be even lower than for the single phase

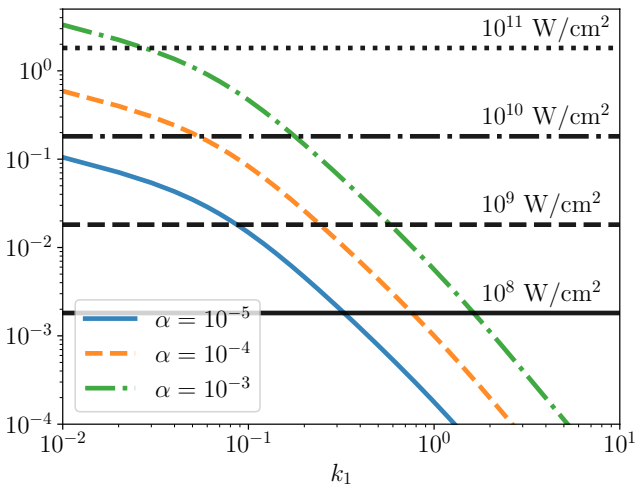

FIG. 9. Approximate thresholds for autoresonant excitation of single phase electron plasma waves. The figure shows the LHS $(I, \lambda = 1\ \mu\text{m}, n_e/n_c = 10^{-3}, T_e = 30\ \text{eV})$ given by Eq. (42) for different values of the laser intensity I [$I = 10^8$ W/cm^2 (solid black), $I = 10^9$ W/cm^2 (dashed black), $I = 10^{10}$ W/cm^2 (dash-dotted black), and $I = 10^{11}$ W/cm^2 (dotted black)] and the RHS (k_1, α) given by Eq. (43) for different values of chirp rate α [$\alpha = 10^{-5}$ (solid blue), $\alpha = 10^{-4}$ (dashed orange), and $\alpha = 10^{-3}$ (dash-dotted green)] as functions of k_1. For the autoresonance to occur, the RHS must be below the horizontal line representing the LHS.

case, because the excited electron density in the "interference" pattern of the two drives can be larger than for the individual drives. Indeed, this can be seen by comparing $\delta n_e/n_e \approx 0.2$ [Figs. 1(b) and 1(c)] for a single phase excitation with $\delta n_e/n_e \approx 0.8$ [Fig. 1(a)] for a two-phase excitation.

Thus, we can expect that the laser intensities on the order of $I \approx 10^{12}$–10^{14} W/cm^2 and the laser duration on the order of $t_{\text{pulse}} \approx 1$–$1000$ ps should be sufficient to autoresonantly drive a single phase ion acoustic wave.

B. Electron plasma waves

Now we can make similar estimates but for the case of electron plasma waves discussed in this paper. In this subsection, all the variables are as they are defined in the current paper.

The single phase threshold condition (36) can again be presented in the form given by Eq. (37), but with the following definitions for the functions LHS and RHS:

$$\text{LHS}\,(I, \lambda, n_e/n_c, T_e) = \frac{U_p\,[\text{eV}]}{m_e\omega_p^2/k^2\,[\text{eV}]}, \tag{42}$$

$$\text{RHS}\,(k_1, \alpha) = 1.644\sqrt{\frac{\omega_1}{2\,|a\,(k_1, \omega_1)|}}\frac{1}{2\,|k_1|}\alpha^{\frac{3}{4}}. \tag{43}$$

Here, U_p is the ponderomotive energy given by Eq. (40). Inside the function RHS (k_1, α) [Eq. (43)] we have the dimensionless wave vector k_1 (measured in k) and the dimensionless frequency ω_1 (measured in units of the electron plasma frequency ω_p) given by the linear plasma wave dispersion relation [Eq. (6)]; the definition of the function $a\,(k_1, \omega_1)$ is from Appendix B, while ω_1, k_1, κ, Δ, and α are as they are defined in this paper.

Figure 9 shows the LHS given by Eq. (42) for different values of the laser intensity I and the RHS given by Eq. (43) for different values of chirp rate α as functions of the dimensionless k_1 (measured in units of k) for $\lambda = 1\ \mu$m, $n_e/n_c = 10^{-3}$, $T_e = 30$ eV, $\kappa = 0.1$. Since we consider in this estimate the threshold for one wave, we measure k_1 in the wave vector of the drive; thus, the relevant value of k_1 is $k_1 = 1$. We see from Fig. 9 that autoresonance should occur if the laser intensity exceeds $I \approx 10^{10}$ W/cm^2 for $\alpha = 10^{-3}$, $I \approx 10^9$ W/cm^2 for $\alpha = 10^{-4}$, and $I \approx 10^8$ W/cm^2 for $\alpha = 10^{-5}$.

As in the case of ion acoustic waves, we can estimate the required laser pulse duration for the autoresonant excitation of electron plasma waves. In the leading linear order, the relative density increase is $(\delta n_e)_1 \approx k_1\widetilde{A}_{10}$. Then, using the asymptotic solution for the effective action $\bar{I}_1 \approx [\alpha/\,|a\,(k_1, \omega_1)|]\,t$ and its connection with $\widetilde{A}_{10}$, we can estimate the dimensionless laser pulse length (measured in units of ω_p^{-1}) required to reach $(\delta n_e/n_e)_1$ as

$$t_{\text{pulse}} = \left[\left(\frac{\delta n_e}{n_e}\right)_1\right]^2 \frac{2\omega_1\,|a\,(k_1, \omega_1)|}{\alpha k_1^2}, \tag{44}$$

where the definition of the function $a\,(k_1, \omega_1)$ is from Appendix B, while ω_1, k_1, κ, Δ, and α are as they are defined in this paper.

Figure 8 plots the pulse length determined by Eq. (44) in picoseconds as a function of chirp rate α for $(\delta n_e/n_e)_1 = 0.25$ (green line with square markers). Other parameters are the same as in Fig. 9, namely $\lambda = 1\ \mu$m, $n_e/n_c = 10^{-3}$, $T_e = 30$ eV, $\kappa = 0.1$. We can see from Fig. 8 that for $\alpha = 10^{-5}$ the laser pulse length of $t_{\text{pulse}} \approx 100$ ps is required, for $\alpha = 10^{-4}$ the pulse length is estimated as $t_{\text{pulse}} \approx 10$ ps, and for $\alpha = 10^{-3}$ the pulse length of $t_{\text{pulse}} \approx 1$ ps should be sufficient.

Thus, we can expect that the laser intensities on the order of $I \approx 10^9$–10^{11} W/cm^2 and the laser duration on the order of $t_{\text{pulse}} \approx 1$–$100$ ps should be sufficient to autoresonantly drive a single phase electron plasma wave.

V. CONCLUSIONS

We have shown how to use phase locking (autoresonance) with small amplitude chirped-frequency ponderomotive drives to create and control strongly nonlinear two-phase plasma waves. The drives can be controlled independently as long as the conditions for the double autoresonance are met. We have illustrated these nonlinear two-phase waves through fully nonlinear numerical

simulations. Using Whitham's averaged Lagrangian procedure we analytically developed a reduced set of ordinary differential equations for the amplitudes and phases of the waves. This analytical weakly nonlinear theory is necessary to understand how to choose the appropriate parameters to drive and control such two-phase structures.

Similar to the case of ion acoustic waves [40], the autoresonantly excited multiphase waves form coherent spatiotemporal quasicrystalline structures, whose properties as accelerating structures and optical elements require further investigation. These nonlinear two-phase structures, have not been seen, to our knowledge, in experiments. The autoresonant excitation described here requires a balance between the pulse amplitude and chirp rate, as given by the threshold, and is also constrained by physics not in our model.

We have made initial estimates for the required laser intensities and pulse lengths. These estimates suggest that the autoresonant method of creating large amplitude coherent structures in plasmas is promising but requires additional investigation. Should the autoresonant method of exciting plasma structures prove to be effective, it would allow for large amplitude structures to be excited with relatively low intensity and energy lasers. First principles models such as particle-in-cell (PIC) simulations will be necessary to further establish the practical aspects of the experimental realization of the autoresonant electron plasma or ion acoustic waves, to gauge the influence of other possible effects (collisional and collisionless damping, various instabilities, higher dimensionality effects, kinetic effects, such as trapping, etc.), and to study their long-term stability.

ACKNOWLEDGMENTS

This work was supported by NSF-BSF Grant No. 1803874 and US-Israel Binational Science Foundation Grant No. 2020233.

Appendix A: The averaged Lagrangian density

The averaged Lagrangian density $\bar{L}$ is the sum of the following terms:

$$\left\langle \frac{1}{2}\varphi_x^2 \right\rangle_{\theta_1,\theta_2} = \frac{1}{4}k_1^2 C_{10}^2 + \frac{1}{4}k_2^2 C_{01}^2 + \frac{1}{4}\left(k_1+k_2\right)^2 C_{11}^2 + \frac{1}{4}\left(k_1-k_2\right)^2 C_{1,-1}^2 + k_1^2 C_{20}^2 + k_2^2 C_{02}^2, \tag{A1}$$

$$\left\langle \frac{1}{2}\kappa^2\varphi^2 \right\rangle_{\theta_1,\theta_2} = \frac{1}{4}\kappa^2 C_{10}^2 + \frac{1}{4}\kappa^2 C_{01}^2 + \frac{1}{4}\kappa^2 C_{11}^2 + \frac{1}{4}\kappa^2 C_{1,-1}^2 + \frac{1}{4}\kappa^2 C_{20}^2 + \frac{1}{4}\kappa^2 C_{02}^2, \tag{A2}$$

$$\begin{aligned}\left\langle -\frac{1}{2}\left(\psi_t\sigma_x + \psi_x\sigma_t\right) \right\rangle_{\theta_1,\theta_2} = {} & \frac{1}{2}\omega_1 k_1 \tilde{B}_{10}\tilde{A}_{10} + \frac{1}{2}\omega_2 k_2 \tilde{B}_{01}\tilde{A}_{01} \\ & + 2\omega_1 k_1 \tilde{B}_{20}\tilde{A}_{20} + 2\omega_2 k_2 \tilde{B}_{02}\tilde{A}_{02} \\ & + \frac{1}{2}\left(\omega_1-\omega_2\right)\left(k_1-k_2\right)\tilde{B}_{1,-1}\tilde{A}_{1,-1} + \frac{1}{2}\left(\omega_1+\omega_2\right)\left(k_1+k_2\right)\tilde{B}_{11}\tilde{A}_{11},\end{aligned} \tag{A3}$$

$$\begin{aligned}\left\langle -\frac{1}{2}\psi_x^2\left(1+\sigma_x\right) \right\rangle_{\theta_1,\theta_2} = {} & -\frac{1}{4}k_1^2\tilde{B}_{10}^2 - \frac{1}{4}k_2^2\tilde{B}_{01}^2 - k_1^2\tilde{B}_{20}^2 - k_2^2\tilde{B}_{02}^2 - \frac{1}{4}\left(k_1+k_2\right)^2\tilde{B}_{11}^2 - \frac{1}{4}\left(k_1-k_2\right)^2\tilde{B}_{1,-1}^2 \\ & - \frac{1}{2}k_2^3\left(\tilde{A}_{01}\tilde{B}_{01}\tilde{B}_{02} + \frac{1}{2}\tilde{A}_{02}\tilde{B}_{01}^2\right) - \frac{1}{2}k_1^3\left(\tilde{A}_{10}\tilde{B}_{10}\tilde{B}_{20} + \frac{1}{2}\tilde{A}_{20}\tilde{B}_{10}^2\right) \\ & - \frac{1}{4}k_1k_2\left(k_1-k_2\right)\left(\tilde{A}_{01}\tilde{B}_{10}\tilde{B}_{1,-1} + \tilde{A}_{1,-1}\tilde{B}_{01}\tilde{B}_{10} + \tilde{A}_{10}\tilde{B}_{01}\tilde{B}_{1,-1}\right) \\ & - \frac{1}{4}k_1k_2\left(k_1+k_2\right)\left(\tilde{A}_{01}\tilde{B}_{11}\tilde{B}_{10} + \tilde{A}_{10}\tilde{B}_{01}\tilde{B}_{11} + \tilde{A}_{11}\tilde{B}_{01}\tilde{B}_{10}\right),\end{aligned} \tag{A4}$$

$$\begin{aligned}\left\langle -\frac{1}{2}\Delta^2\sigma_x^2\left(1+\frac{1}{3}\sigma_x\right) \right\rangle_{\theta_1,\theta_2} = {} & -\frac{1}{4}\Delta^2 k_1^2\tilde{A}_{10}^2 - \frac{1}{4}\Delta^2 k_1^3\tilde{A}_{10}^2\tilde{A}_{20} - \Delta^2 k_1^2\tilde{A}_{20}^2 - \frac{1}{4}\Delta^2 k_2^2\tilde{A}_{01}^2 - \frac{1}{4}\Delta^2 k_2^3\tilde{A}_{01}^2\tilde{A}_{02} - \Delta^2 k_2^2\tilde{A}_{02}^2 \\ & - \frac{1}{4}\Delta^2 k_1k_2\left(k_1-k_2\right)\tilde{A}_{01}\tilde{A}_{10}\tilde{A}_{1,-1} - \frac{1}{4}\Delta^2 k_1k_2\left(k_1+k_2\right)\tilde{A}_{01}\tilde{A}_{10}\tilde{A}_{11} - \frac{1}{4}\Delta^2\left(k_1-k_2\right)^2\tilde{A}_{1,-1}^2 - \frac{1}{4}\Delta^2\left(k_1+k_2\right)^2\tilde{A}_{11}^2,\end{aligned} \tag{A5}$$

$$\langle\sigma_x\varphi\rangle_{\theta_1,\theta_2}=\frac{1}{2}k_1\tilde{A}_{10}C_{10}+\frac{1}{2}k_2\tilde{A}_{01}C_{01}+\frac{1}{2}\left(k_1+k_2\right)\tilde{A}_{11}C_{11}+\frac{1}{2}\left(k_1-k_2\right)\tilde{A}_{1,-1}C_{1,-1}+k_1\tilde{A}_{20}C_{20}+k_2\tilde{A}_{02}C_{02}, \quad \text{(A6)}$$

$$\langle\sigma_x\varphi_d\rangle_{\theta_1,\theta_2}=\frac{1}{2}\varepsilon_1k_1\tilde{A}_{10}\cos\left(\Phi_1\right)+\frac{1}{2}\varepsilon_2k_2\tilde{A}_{01}\cos\left(\Phi_2\right). \quad \text{(A7)}$$

Appendix B: Functions $a\left(k_1,\omega_1\right)$, $b\left(k_1,\omega_1;k_2,\omega_2\right)$, and $c\left(k_2,\omega_2\right)$

The function $a\left(k_1,\omega_1\right)$ is defined via

$$C_{10}^2a\left(k_1,\omega_1\right)=-\frac{1}{2\omega_1\left(1+\frac{\kappa^2}{k_1^2}\right)^2}\tilde{B}_{20}-\frac{\omega_1^2+\Delta^2k_1^2}{4\omega_1^2k_1\left(1+\frac{\kappa^2}{k_1^2}\right)^2}\tilde{A}_{20}, \quad \text{(B1)}$$

The function $c\left(k_2,\omega_2\right)$ is defined via

$$C_{01}^2c\left(k_2,\omega_2\right)=-\frac{1}{2\omega_2\left(1+\frac{\kappa^2}{k_2^2}\right)^2}\tilde{B}_{02}-\frac{\omega_2^2+\Delta^2k_2^2}{4\omega_2^2k_2\left(1+\frac{\kappa^2}{k_2^2}\right)^2}\tilde{A}_{02}, \quad \text{(B2)}$$

where we note that, due to symmetry, the functions $a\left(k_1,\omega_1\right)$ and $c\left(k_2,\omega_2\right)$ should have an identical functional dependence.

The function $b\left(k_1,\omega_1;k_2,\omega_2\right)$ is defined via

$$\begin{aligned}C_{10}C_{01}b\left(k_1,\omega_1;k_2,\omega_2\right)=&-\frac{\omega_1\omega_2+\Delta^2k_1k_2}{8\omega_1\omega_2k_1k_2\left(1+\frac{\kappa^2}{k_1^2}\right)\left(1+\frac{\kappa^2}{k_2^2}\right)}\left[\left(k_1-k_2\right)\tilde{A}_{1,-1}+\left(k_1+k_2\right)\tilde{A}_{11}\right]\\&-\frac{\omega_1k_2+\omega_2k_1}{8\omega_1\omega_2k_1k_2\left(1+\frac{\kappa^2}{k_1^2}\right)\left(1+\frac{\kappa^2}{k_2^2}\right)}\left[\left(k_1-k_2\right)\tilde{B}_{1,-1}+\left(k_1+k_2\right)\tilde{B}_{11}\right]. \quad \text{(B3)}\end{aligned}$$

Here, the amplitudes $\tilde{A}_{20}$, $\tilde{A}_{02}$, $\tilde{B}_{20}$, $\tilde{B}_{02}$, C_{20}, C_{02}, $\tilde{A}_{11}$, $\tilde{A}_{1,-1}$, $\tilde{B}_{11}$, $\tilde{B}_{1,-1}$, C_{11}, $C_{1,-1}$ should be expressed through C_{10}, C_{01}, k_1, k_2, ω_1, ω_2, κ, Δ using Eqs. (C1)–(C12) of Appendix C, so that $a\left(k_1,\omega_1\right)$, $b\left(k_1,\omega_1;k_2,\omega_2\right)$, and $c\left(k_2,\omega_2\right)$ are functions of k_1, k_2, ω_1, ω_2, κ, Δ only. The dimensionless frequencies ω_1 and ω_2 are determined by the linear plasma wave dispersion relation [Eq. (6)].

Appendix C: The second-order amplitudes

To express the second-order amplitudes through the first-order amplitudes C_{10} and C_{01}, we calculate the variations of the averaged Lagrangian density $\bar{L}$ with respect to the second-order amplitudes and, after solving the resulting system of equations and using the linear relations (16)–(19), we obtain the expressions for the second-order amplitudes.

From variations with respect to $\tilde{A}_{20}$, $\tilde{A}_{02}$, $\tilde{B}_{20}$, $\tilde{B}_{02}$, C_{20}, C_{02} and the linear relations (16)–(19), we obtain

$$\tilde{A}_{20}=-k_1^3\left(4+\frac{\kappa^2}{k_1^2}\right)\left(1+\frac{\kappa^2}{k_1^2}\right)^2\frac{3\omega_1^2+\Delta^2k_1^2}{8\left[1-\left(\omega_1^2-\Delta^2k_1^2\right)\left(4+\frac{\kappa^2}{k_1^2}\right)\right]}C_{10}^2, \quad \text{(C1)}$$

$$\tilde{A}_{02}=-k_2^3\left(4+\frac{\kappa^2}{k_2^2}\right)\left(1+\frac{\kappa^2}{k_2^2}\right)^2\frac{3\omega_2^2+\Delta^2k_2^2}{8\left[1-\left(\omega_2^2-\Delta^2k_2^2\right)\left(4+\frac{\kappa^2}{k_2^2}\right)\right]}C_{01}^2, \quad \text{(C2)}$$

$$\tilde{B}_{20}=-\omega_1k_1^2\left(1+\frac{\kappa^2}{k_1^2}\right)^2\frac{2+\left(\omega_1^2+3\Delta^2k_1^2\right)\left(4+\frac{\kappa^2}{k_1^2}\right)}{8\left[1-\left(\omega_1^2-\Delta^2k_1^2\right)\left(4+\frac{\kappa^2}{k_1^2}\right)\right]}C_{10}^2, \quad \text{(C3)}$$

$$\tilde{B}_{02}=-\omega_2k_2^2\left(1+\frac{\kappa^2}{k_2^2}\right)^2\frac{2+\left(\omega_2^2+3\Delta^2k_2^2\right)\left(4+\frac{\kappa^2}{k_2^2}\right)}{8\left[1-\left(\omega_2^2-\Delta^2k_2^2\right)\left(4+\frac{\kappa^2}{k_2^2}\right)\right]}C_{01}^2, \quad \text{(C4)}$$

$$C_{20} = k_1^2 \left(1+\frac{\kappa^2}{k_1^2}\right)^2 \frac{3\omega_1^2+\Delta^2 k_1^2}{4\left[1-\left(\omega_1^2-\Delta^2 k_1^2\right)\left(4+\frac{\kappa^2}{k_1^2}\right)\right]} C_{10}^2, \tag{C5}$$

$$C_{02} = k_2^2 \left(1+\frac{\kappa^2}{k_2^2}\right)^2 \frac{3\omega_2^2+\Delta^2 k_2^2}{4\left[1-\left(\omega_2^2-\Delta^2 k_2^2\right)\left(4+\frac{\kappa^2}{k_2^2}\right)\right]} C_{01}^2. \tag{C6}$$

From variations with respect to $\tilde{A}_{11}$, $\tilde{A}_{1,-1}$, $\tilde{B}_{11}$, $\tilde{B}_{1,-1}$, C_{11}, $C_{1,-1}$ and the linear relations (16)–(19), we obtain

$$\tilde{A}_{11} = k_1 k_2 \left(1+\frac{\kappa^2}{k_1^2}\right)\left(1+\frac{\kappa^2}{k_2^2}\right) \frac{\left[(k_1+k_2)^2+\kappa^2\right]\left[(k_1+k_2)\left(\omega_1\omega_2+\Delta^2 k_1 k_2\right)+(\omega_1+\omega_2)\left(\omega_1 k_2+\omega_2 k_1\right)\right]}{2\left\{\left[(\omega_1+\omega_2)^2-\Delta^2\left(k_1+k_2\right)^2\right]\left[(k_1+k_2)^2+\kappa^2\right]-(k_1+k_2)^2\right\}} C_{10}C_{01}, \tag{C7}$$

$$\tilde{A}_{1,-1} = k_1 k_2 \left(1+\frac{\kappa^2}{k_1^2}\right)\left(1+\frac{\kappa^2}{k_2^2}\right) \frac{\left[(k_1-k_2)^2+\kappa^2\right]\left[(k_1-k_2)\left(\omega_1\omega_2+\Delta^2 k_1 k_2\right)+(\omega_1-\omega_2)\left(\omega_1 k_2+\omega_2 k_1\right)\right]}{2\left\{\left[(\omega_1-\omega_2)^2-\Delta^2\left(k_1-k_2\right)^2\right]\left[(k_1-k_2)^2+\kappa^2\right]-(k_1-k_2)^2\right\}} C_{10}C_{01}, \tag{C8}$$

$$\begin{aligned}\tilde{B}_{11} = {} & k_1 k_2 \left(1+\frac{\kappa^2}{k_1^2}\right)\left(1+\frac{\kappa^2}{k_2^2}\right) \frac{(\omega_1+\omega_2)\left[(k_1+k_2)^2+\kappa^2\right]\left(\omega_1\omega_2+\Delta^2 k_1 k_2\right)}{2\left\{\left[(\omega_1+\omega_2)^2-\Delta^2\left(k_1+k_2\right)^2\right]\left[(k_1+k_2)^2+\kappa^2\right]-(k_1+k_2)^2\right\}} C_{10}C_{01} \\ & + k_1 k_2 \left(1+\frac{\kappa^2}{k_1^2}\right)\left(1+\frac{\kappa^2}{k_2^2}\right) \frac{(k_1+k_2)\left\{1+\Delta^2\left[(k_1+k_2)^2+\kappa^2\right]\right\}\left(\omega_1 k_2+\omega_2 k_1\right)}{2\left\{\left[(\omega_1+\omega_2)^2-\Delta^2\left(k_1+k_2\right)^2\right]\left[(k_1+k_2)^2+\kappa^2\right]-(k_1+k_2)^2\right\}} C_{10}C_{01},\end{aligned} \tag{C9}$$

$$\begin{aligned}\tilde{B}_{1,-1} = {} & k_1 k_2 \left(1+\frac{\kappa^2}{k_1^2}\right)\left(1+\frac{\kappa^2}{k_2^2}\right) \frac{(\omega_1-\omega_2)\left[(k_1-k_2)^2+\kappa^2\right]\left(\omega_1\omega_2+\Delta^2 k_1 k_2\right)}{2\left\{\left[(\omega_1-\omega_2)^2-\Delta^2\left(k_1-k_2\right)^2\right]\left[(k_1-k_2)^2+\kappa^2\right]-(k_1-k_2)^2\right\}} C_{10}C_{01} \\ & + k_1 k_2 \left(1+\frac{\kappa^2}{k_1^2}\right)\left(1+\frac{\kappa^2}{k_2^2}\right) \frac{(k_1-k_2)\left\{1+\Delta^2\left[(k_1-k_2)^2+\kappa^2\right]\right\}\left(\omega_1 k_2+\omega_2 k_1\right)}{2\left\{\left[(\omega_1-\omega_2)^2-\Delta^2\left(k_1-k_2\right)^2\right]\left[(k_1-k_2)^2+\kappa^2\right]-(k_1-k_2)^2\right\}} C_{10}C_{01},\end{aligned} \tag{C10}$$

$$C_{11} = -k_1 k_2 \left(1+\frac{\kappa^2}{k_1^2}\right)\left(1+\frac{\kappa^2}{k_2^2}\right) \frac{(k_1+k_2)\left[(k_1+k_2)\left(\omega_1\omega_2+\Delta^2 k_1 k_2\right)+(\omega_1+\omega_2)\left(\omega_1 k_2+\omega_2 k_1\right)\right]}{2\left\{\left[(\omega_1+\omega_2)^2-\Delta^2\left(k_1+k_2\right)^2\right]\left[(k_1+k_2)^2+\kappa^2\right]-(k_1+k_2)^2\right\}} C_{10}C_{01}, \tag{C11}$$

$$C_{1,-1} = -k_1 k_2 \left(1+\frac{\kappa^2}{k_1^2}\right)\left(1+\frac{\kappa^2}{k_2^2}\right) \frac{(k_1-k_2)\left[(k_1-k_2)\left(\omega_1\omega_2+\Delta^2 k_1 k_2\right)+(\omega_1-\omega_2)\left(\omega_1 k_2+\omega_2 k_1\right)\right]}{2\left\{\left[(\omega_1-\omega_2)^2-\Delta^2\left(k_1-k_2\right)^2\right]\left[(k_1-k_2)^2+\kappa^2\right]-(k_1-k_2)^2\right\}} C_{10}C_{01}. \tag{C12}$$

[1] F. Einaudi and R. N. Sudan, Phys. Plasmas **11**, 359 (1969).
[2] W. M. Manheimer, Phys. Fluids **12**, 2426 (1969).
[3] T. P. Coffey, Phys. Fluids **14**, 1402 (1971).
[4] G. J. Morales and T. M. O'Neil, Phys. Rev. Lett. **28**, 417 (1972).
[5] R. L. Dewar, Phys. Fluids **15**, 712 (1972).
[6] R. L. Dewar and J. Lindl, Phys. Fluids **15**, 820 (1972).
[7] B. I. Cohen and A. N. Kaufman, Phys. Fluids **20**, 1113 (1977).
[8] R. R. Lindberg, A. E. Charman, and J. S. Wurtele, Phys. Plasmas **14**, 122103 (2007).

[9] I. Y. Dodin and N. J. Fisch, Phys. Rev. Lett. **107**, 035005 (2011).
[10] R. L. Berger, S. Brunner, T. Chapman, L. Divol, C. H. Still, and E. J. Valeo, Phys. Plasmas **20**, 032107 (2013).
[11] D. Bénisti, Phys. Plasmas **23**, 102105 (2016).
[12] D. H. E. Dubin and A. Ashourvan, Phys. Plasmas **22**, 102102 (2015).
[13] C. Liu and I. Y. Dodin, Phys. Plasmas **22**, 082117 (2015).
[14] M. Tacu and D. Bénisti, Phys. Plasmas **29**, 052108 (2022).
[15] D. Bénisti, D. F. G. Minenna, M. Tacu, A. Debayle, and L. Gremillet, Phys. Plasmas **29**, 052109 (2022).
[16] B. J. Winjum, J. Fahlen, and W. B. Mori, Phys. Plasmas **14**, 102104 (2007).
[17] T. Tajima and J. M. Dawson, Phys. Rev. Lett. **43**, 267 (1979).
[18] W. L. Kruer, in *Laser Plasma Interactions 5*, edited by M. B. Hooper (CRC Press, New York, 1995) pp. 27–44.
[19] H. Milchberg, Phys. Today **72**, 70 (2019).
[20] G. Lehmann and K. H. Spatschek, Phys. Rev. Lett. **116**, 225002 (2016).
[21] M. R. Edwards, V. R. Munirov, A. Singh, N. M. Fasano, E. Kur, N. Lemos, J. M. Mikhailova, J. S. Wurtele, and P. Michel, Phys. Rev. Lett. **128**, 065003 (2022).
[22] P. Michel, L. Divol, D. Turnbull, and J. D. Moody, Phys. Rev. Lett. **113**, 205001 (2014).
[23] D. Turnbull, P. Michel, T. Chapman, E. Tubman, B. B. Pollock, C. Y. Chen, C. Goyon, J. S. Ross, L. Divol, N. Woolsey, and J. D. Moody, Phys. Rev. Lett. **116**, 205001 (2016).
[24] G. Lehmann and K. H. Spatschek, Phys. Rev. E **97**, 063201 (2018).
[25] E. Kur, M. Lazarow, J. S. Wurtele, and P. Michel, Opt. Express **29**, 1162 (2021).
[26] V. M. Malkin, G. Shvets, and N. J. Fisch, Phys. Rev. Lett. **82**, 4448 (1999).
[27] P. Michel, L. Divol, E. A. Williams, S. Weber, C. A. Thomas, D. A. Callahan, S. W. Haan, J. D. Salmonson, S. Dixit, D. E. Hinkel, M. J. Edwards, B. J. MacGowan, J. D. Lindl, S. H. Glenzer, and L. J. Suter, Phys. Rev. Lett. **102**, 025004 (2009).
[28] J. Fajans and L. Friedland, Am. J. Phys. **69**, 1096 (2001).
[29] L. Friedland, Scholarpedia **4**, 5473 (2009).
[30] R. R. Lindberg, A. E. Charman, J. S. Wurtele, and L. Friedland, Phys. Rev. Lett. **93**, 055001 (2004).
[31] O. Yaakobi, L. Friedland, R. R. Lindberg, A. E. Charman, G. Penn, and J. S. Wurtele, Phys. Plasmas **15**, 032105 (2008).
[32] L. Friedland and A. G. Shagalov, Phys. Rev. E **89**, 053103 (2014).
[33] L. Friedland and A. G. Shagalov, Phys. Plasmas **24**, 082106 (2017).
[34] L. Friedland, G. Marcus, J. S. Wurtele, and P. Michel, Phys. Plasmas **26**, 092109 (2019).
[35] L. Friedland and A. G. Shagalov, J. Plasma Phys. **86**, 825860301 (2020).
[36] L. Friedland and A. G. Shagalov, Phys. Rev. Lett. **90**, 074101 (2003).
[37] M. Khasin and L. Friedland, Phys. Rev. E **68**, 066214 (2003).
[38] L. Friedland and A. G. Shagalov, Phys. Rev. E **71**, 036206 (2005).
[39] A. Shagalov and L. Friedland, Physica D **238**, 1561 (2009).
[40] V. R. Munirov, L. Friedland, and J. S. Wurtele, Phys. Rev. Research **4**, 023150 (2022).
[41] G. B. Whitham, J. Fluid Mech. **22**, 273 (1965).
[42] G. B. Whitham, *Linear and nonlinear waves* (Wiley, New York, 1999).
[43] C. Canuto, M. Yousuff Hussaini, A. Quarteroni, and Z. Thomas A., Jr, *Spectral methods in fluid dynamics*, Scientific Computation (Springer, Berlin, Germany, 1988).
[44] M. Buchanan and J. J. Dorning, Phys. Rev. Lett. **70**, 3732 (1993).
[45] I. Barth and L. Friedland, Phys. Rev. E **76**, 016211 (2007).